

## Supporting Information

### **The first zeolite with a tri-directional extra-large 14-ring pore system derived using a phosphonium-based organic molecule**

Yifeng Yun, ‡<sup>a</sup> Manuel Hernández, ‡<sup>b</sup> Wei Wan,<sup>a</sup> Xiaodong Zou,<sup>\*a</sup> Jose L. Jordá,<sup>b</sup> Angel Cantín,<sup>b</sup> Fernando Rey,<sup>b</sup> Avelino Corma<sup>\*b</sup>

<sup>a</sup> Berzelii Center EXSELENT on Porous Materials and Inorganic and Structural Chemistry, Department of Materials and Environmental Chemistry, Stockholm University, SE-106 91 Stockholm, Sweden

<sup>b</sup> DepartmeInstituto de Tecnología Química (UPV-CSIC), Universidad Politécnica de Valencia - Consejo Superior de Investigaciones Científicas, Av. de los Naranjos s/n, 46022 Valencia, Spain

E-mail: xzou@mmk.su.se

E-mail: acorma@itq.upv.es

‡ These authors contributed equally to this work.

### Contents

- S1. Synthesis of the organic structure directing agents (OSDAs)
- S2. Synthesis of ITQ-53
- S3. Chemical and elemental analyses of ITQ-53
- S4. Textural properties of ITQ-53
- S5. Solid state MAS-NMR of the ITQ-53 samples
- S6. Structure determination of ITQ-53 and a SAS-type zeolite using RED
- S7. Rietveld refinement against PXRD data of as-synthesised and calcined ITQ-53
- S8. Topology analysis of the ITQ-53 framework

## **S1. Synthesis of the Organic Structure Directing Agent (OSDA) hydroxide [tri-tertbutylmethylphosphonium hydroxide]**

A solution of tri-tertbutylphosphine (20 g, 96.9 mmol) in ethylacetate (200 mL) was placed in a 500 mL three-necked vial. Iodomethane (9.1 mL, 145 mmol diluted in 50 ml of ethylacetate) was added dropwise over the solution through a dropping funnel in an ice bath. After the complete addition of the alkyl iodide, the ice bath assembly was removed. The reaction system was under inert atmosphere ( $N_2$ ) during all the reaction time.

The reaction mixture was stirred at room temperature for one day, and then filtered. The solid product was washed with ethyl acetate and diethyl ether, dried under vacuum for 4 hours to give 32.7 g solid (the reaction yield was 98%).

Finally, the solid was dissolved in water and exchanged to its hydroxide form at room temperature overnight using a Dowex SBR anionic exchange resin in batch. The aqueous solution of OSDA(OH) was rotaevaporated until reaching a concentration of nearly 0.75 M of the OSDA(OH).

## **S2. Synthesis of ITQ-53 zeolite**

For a typical synthesis of the zeolite ITQ-53, 2.09 g of germanium oxide (20.0 mmol, >99.5 % Aldrich) and 4.16 g of tetraethylorthosilicate (20.0 mmol, TEOS, >99 %, Aldrich) were added to 26.70 g of the aqueous OSDA(OH) solution (0.75 M, 20.0 mmol).

The mixture was stirred at room temperature until a total evaporation of the ethanol formed during the hydrolysis of TEOS. Then, 0.833 g of 48 wt% hydrofluoric acid (20 mmol, Aldrich) was added, and finally water was added to adjust the  $H_2O/(Si+Ge)$  ratio to 7.0. The final synthesis gel composition was:



The resulting gel was placed in Teflon-lined steel autoclaves and kept at 150 °C under tumbling for 14 hours. After cooling, the solid was recovered by filtration, washed with hot water, and dried at 100 °C overnight to obtain the as-synthesised zeolite ITQ-53.

The synthesis conditions given above were the optimised ones. A series of synthesis parameters were tested before pure OTQ-53 could be synthesised. The synthesis gel given above was tested in a range of temperatures and crystallisation times (Table S1). At low temperature (135 °C) the synthesis yielded a mixture of ITQ-53 and the SAS-type zeolite (STA-6 or SSZ-73), while at high temperature (175 °C) the only product was the dense germanium dioxide phase. At 150 °C, however, pure ITQ-53 was obtained. ITQ-53 seems to be a dynamically stable phase at 150 °C, being obtained in half a day, and remained the only product even after 4 days.

**Table S1.** Temperatures and synthesis times tested for the synthesis of ITQ-53.

T (° C)	t (days)	Phase
135	4	ITQ-53 + SAS
135	5	ITQ-53 + SAS
150	0.5	ITQ-53
150	3	ITQ-53
150	4	ITQ-53
175	1	GeO <sub>2</sub>
175	3	GeO <sub>2</sub>

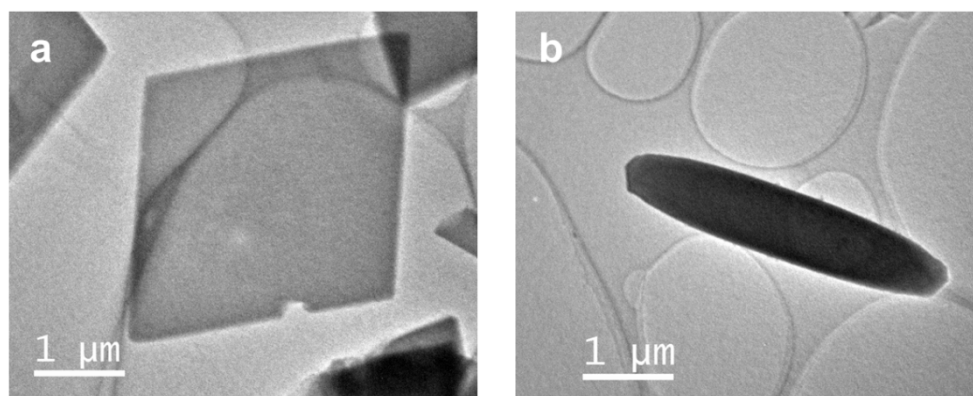


**Figure S1.** TEM images showing (a) the plate-like ITQ-53 crystal and (b) the rod-like SAS-type crystal in the initially-synthesised ITQ-53 sample.

### S3. Chemical and elemental analyses of the zeolite ITQ-53

The results of chemical and elemental analyses of the as-synthesised pure ITQ-53 sample are given in Table S2. The chemical analysis gave a Si/Ge ratio of 1.1, similar to the gel composition (Si/Ge = 1.0). The (Si+Ge)/P ratio was 9.6, corresponding to 16 OSDA molecules per unit cell. The elemental analysis showed a C/P ratio of 14.1, which is close to that of the pure OSDA (13.0). This indicates that the OSDA remained intact during the synthesis.

**Table S2.** The results of chemical and elemental analyses of the as-synthesised zeolite ITQ-53.

	In wt%					In molar ratio			
	Si	Ge	P	F	C	Si/Ge	C/P	P/F	(Si+Ge)/P
Observed	13.45	31.29	2.93	0.99	15.98	1.1	14.1	1.8	9.6
Calculated	13.56	32.39	3.03	0.93	15.26	1.1	13.0	2.0	9.5

#### S4. Textural properties of ITQ-53

N<sub>2</sub> sorption and Ar sorption experiments of the calcined zeolite ITQ-53 were performed on a Micromeritics ASAP 2420 and a Micromeritics ASAP 2020, respectively. Upon zeolite calcination at 400 °C in dry air, the BET surface area and the total micropore volume of ITQ-53 (calculated from the N<sub>2</sub> adsorption isotherm by applying the t-plot method) were 533 m<sup>2</sup>/g and 0.22 cm<sup>3</sup>/g, respectively. The micropore distribution calculated by applying the Hovarth-Kawazoe formalism to the Ar adsorption isotherm showed a maximum at 8.1 Å (Fig. S2).

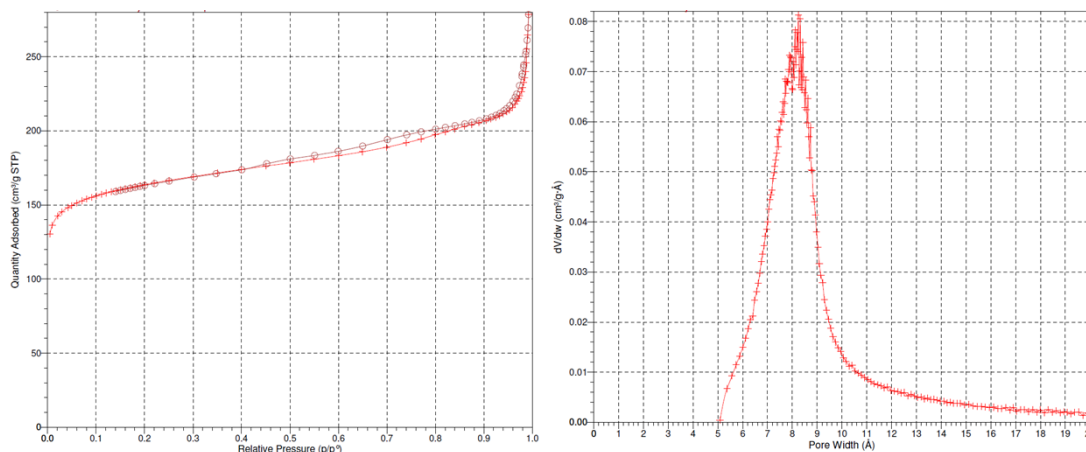


**Figure S2.** Textural properties of zeolite ITQ-53. Left: N<sub>2</sub> sorption isotherm at 77 K. Right: Pore diameter distribution determined from the Ar adsorption isotherm at 87 K.

#### S5. Solid state MAS-NMR of the ITQ-53 samples

The <sup>13</sup>C MAS-NMR and the <sup>31</sup>P MAS-NMR spectra of the as-synthesised ITQ-53 show that the phosphorus-containing OSDA is intact in the sample (Fig. S3), which was also suggested by the chemical analysis (Table S2).

The <sup>13</sup>C MAS-NMR spectrum presents the same number of signals than that of the original OSDA in solution, at almost the same chemical shifts. The <sup>31</sup>P MAS-NMR spectrum shows one band at 50.0 ppm, coincident with that of the OSDA in solution (at 50.1 ppm), but presents also a second band at 48.3 ppm. This second signal can be due to a second location of the OSDA in the channels, producing a different interaction between the P atom and the corresponding counter-ion.

The <sup>19</sup>F MAS-NMR spectrum of the as-synthesised material shows a single resonance at -8.8 ppm (Fig. S4). This resonance can be attributed to F<sup>-</sup> anions located in D4R units.

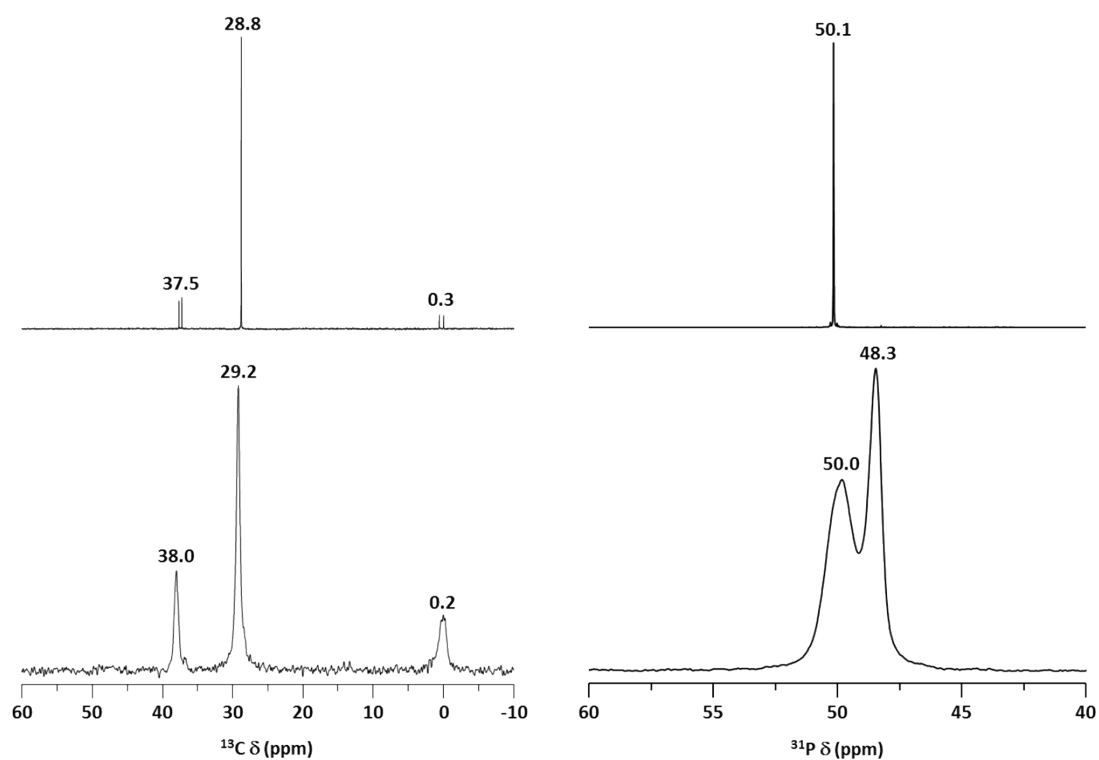


**Figure S3.** (Left) Liquid  $^{13}\text{C}$  NMR spectrum of the OSDA in deuterated water (top) and solid state  $^{13}\text{C}$  MAS-NMR spectrum of the as-synthesised ITQ-53 (bottom). (Right) Liquid  $^{31}\text{P}$  NMR spectrum of the pure OSDA in deuterated water (top) and solid state  $^{31}\text{P}$  MAS-NMR spectrum of the as-synthesised ITQ-53 (bottom).

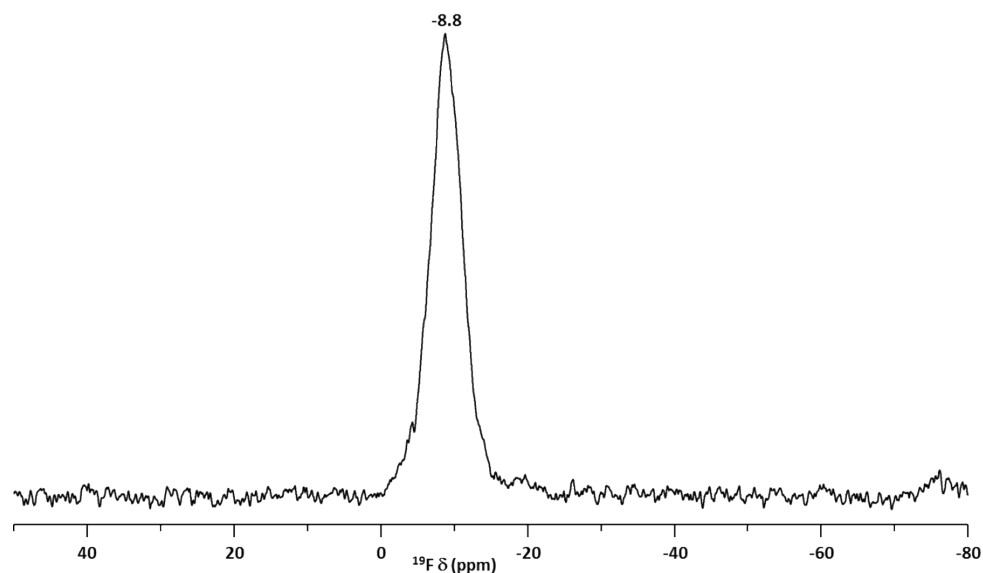


**Figure S4.**  $^{19}\text{F}$  MAS-NMR spectra of the as-synthesised ITQ-53.

## S6. Structure determination of ITQ-53 and the SAS-type zeolite by RED

The powders of initially-synthesised ITQ-53 sample were crushed, dispersed in absolute ethanol and treated by sonication for one minute. Then, a droplet of the suspension was transferred onto a copper grid covered with carbon film. The TEM sample was observed on a JEOL JEM-2100 microscope operated at 200 kV using a single-tilt tomography sample holder. 460 ED frames, with a tilt range of  $84.36^\circ$  and a tilt step of  $0.20^\circ$ , were recorded in selected area electron diffraction (SAED) mode on a 12-bit Gatan ES500W Erlangshen camera side-mounted at a 35 mm port. The *RED* data collection and processing software<sup>1</sup> was used for three-dimensional electron diffraction (ED) data collection and process, respectively.

The 2D SAED frames were combined to reconstruct the three-dimensional reciprocal lattices using the software *RED* – data processing, which includes shift correction, peak search, unit cell determination, indexation of reflections and intensity extraction. The maximum intensity value for each detected reflection was used, while intensities of reflections that cannot be detected by peak hunting were assigned as 0.0. A list of hkl intensity was extracted from RED data and used for structure solution by direct methods using the SHELXS-97 program<sup>2</sup>. A significant electron beam damage of the crystals was observed during the data collection. Thus, the maximum intensities of the symmetry-related reflections were used for the structure refinement instead of the symmetry-averaged intensities.

Two different phases were found in the initially synthesised ITQ-53 samples, ITQ-53 and a SAS-type phase. Details of the 3D-RED data collection and crystal data of ITQ-53 and the SAS-type phase are given in Tables S3 and S4, respectively. The reciprocal lattice of the SAS-type phase reconstructed from the RED data is shown in Fig. S5.

**Table S3.** 3D-RED data collection, crystal data and structure refinement details of ITQ-53 (resolution cut to 1.20 Å).

Tilt angle	+ 53.80 ° to – 30.56°
Tilt step	0.2°
No. of RED frames	460
Exposure time/frame	1.5 s
<i>a</i> / Å	19.12
<i>b</i> / Å	22.77
<i>c</i> / Å	30.21
$\alpha$ / °	90.91
$\beta$ / °	90.94
$\gamma$ / °	90.25
Space group	<i>Cmcm</i>
Completeness	0.786
$R_{\text{int}}$	0.546
No. of measured reflections	7125
No. of independent reflections	1714
<i>h</i>	$-15 \leq h \leq 15$
<i>k</i>	$-18 \leq k \leq 18$
<i>l</i>	$-21 \leq l \leq 21$
$R1^1$	0.451
No. of parameters	130
No. of restraints	62

<sup>1</sup> The structure refinement was based on the structure model with Si atoms in all the T-sites. The occupancy of Si/Ge at each position could not be refined.

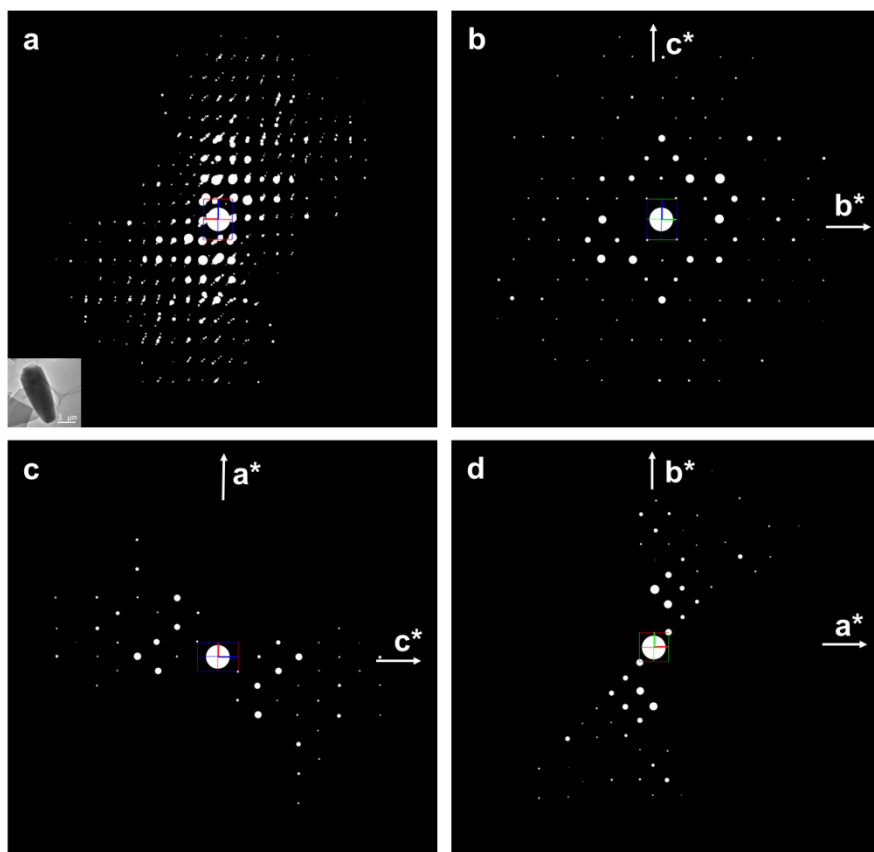


**Figure S5.** (a) 3D reciprocal lattice of SAS reconstructed from the RED data. The crystal from which the RED data was collected is inserted. (b-d)  $(0kl)$  (b),  $(h0l)$  (c) and  $(hk0)$  (d) planes cut from (a). The reflection conditions can be deduced from the RED data as  $hkl$ :  $h + k + l = 2n$ ,  $0kl$ :  $k + l = 2n$ ,  $h0l$ :  $h + l = 2n$ ,  $hk0$ :  $h + k = 2n$ ,  $h00$ :  $h = 2n$ ,  $0k0$ :  $k = 2n$  and  $00l$ :  $l = 2n$ . The possible space groups are  $I222$ ,  $I2_12_12_1$ ,  $Imm2$  and  $Immm$ .

**Table S4.** 3D-RED data collection, crystal data and structure refinement details of a SAS-type phase (resolution cut to 1.15 Å).

Tilt angle	+ 51.27° to – 43.54°
Tilt step	0.2°
No. of RED frames	517
Exposure time/frame	3.0 s
<i>a</i> / Å	14.28
<i>b</i> / Å	14.00
<i>c</i> / Å	10.17
$\alpha$ / °	90.38
$\beta$ / °	89.98
$\gamma$ / °	90.07
Space group	<i>Immm</i>
Completeness	0.883
<i>R</i> <sub>int</sub>	0.374
No. of measured reflections	1447
No. of independent reflections	379
<i>h</i>	-11 ≤ <i>h</i> ≤ 11
<i>k</i>	-12 ≤ <i>k</i> ≤ 12
<i>l</i>	-8 ≤ <i>l</i> ≤ 8
<i>R</i> <sub>1</sub> <sup>1</sup>	0.335
No. of parameters	33
No. of restraints	12

<sup>1</sup> The structure refinement was based on the structure model with Si atoms in all the T-sites. The occupancy of Si/Ge at each position could not be refined.

## S7. Rietveld refinement of as-synthesised and calcined ITQ-53 against the PXRD data

Powder X-ray diffraction data of the as-synthesised ITQ-53 sample were collected in a Anton Paar XRK-900 chamber attached to a PANalytical X-Pert Pro diffractometer using Bragg-Brentano geometry, with Cu K $\alpha$  radiation (45 kV, 40 mA) and an X'Celerator detector.

The monoclinic model was refined against the PXRD data of the as-synthesised ITQ-53 by Rietveld refinement using TOPAS Academic V4.1<sup>3</sup> with soft restraints for the T-O bond distances and O-T-O angles. Two unique F atoms were added manually in the D4Rs obtained from the <sup>19</sup>F NMR (Fig. S4). All the T positions were refined with mixed occupancies of Si and Ge with a fixed overall Si/Ge ratio of 1.1. Rigid body restraints were applied to OSDAs. Two unique OSDAs were added according to the elemental analysis and <sup>31</sup>P NMR spectrum. One guest water molecule and one hydroxyl OH<sup>-</sup> group were added based on the residual electron densities in the difference Fourier maps and also considering the charge balance. The final refinement converged to  $R_B = 1.89\%$ ,  $R_{wp} = 6.86\%$  and  $R_{exp} = 2.55\%$ , as given in Table S5.

**Table S5.** Crystallographic data for Rietveld refinement of as-synthesised ITQ-53.

Chemical formula/unit cell	$[(C_{13}PH_{30})_{16}(OH)_8(H_2O)_8][Si_{79.01}Ge_{72.99}O_{300}(OH)_8F_8]$
Formula weight	16366.35 g/mol
<i>a</i>	18.9248(9) Å
<i>b</i>	22.8167(10) Å
<i>c</i>	30.3099(9) Å
$\beta$	90.8819(40) °
<i>V</i>	13086.28(91) Å <sup>3</sup>
Space group	<i>C2/c</i> (No.15)
Wavelength	1.5418 Å
No. of reflections	3439
No. of parameters	331
No. of restraints	76 T-O distances (Ge-O=1.74 Å, Si-O=1.61 Å) 117 O-O distances (related to the occupancies of Si/Ge at each position) Si/Ge = 1.10 Rigid body for OSDAs
$R_p$	0.0516
$R_{wp}$	0.0686
$R_{exp}$	0.0255
$R_B$	0.0189
GOF	2.69

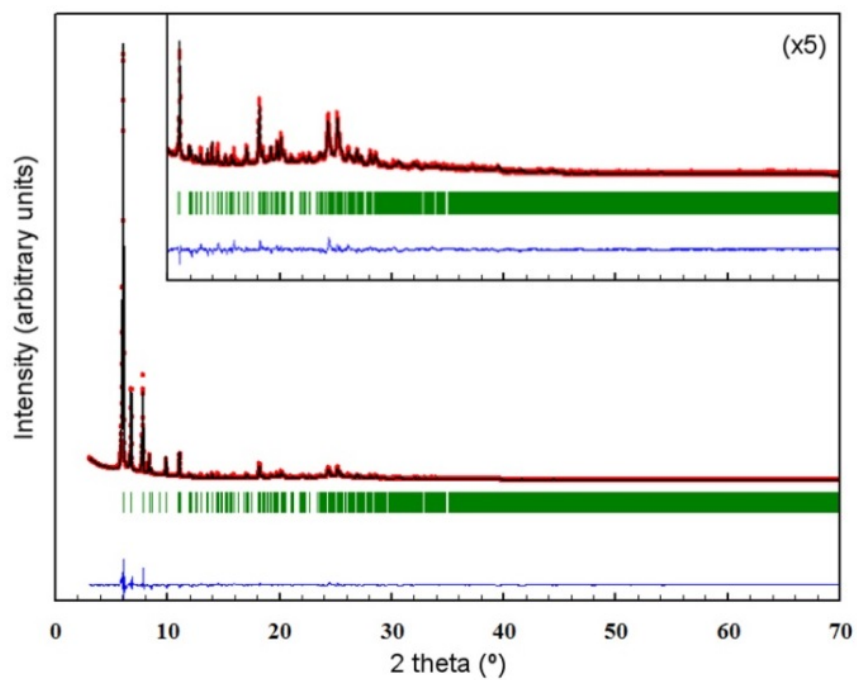


**Figure S6.** Rietveld refinement of the PXRD pattern of calcined ITQ-53 (data collected at 303 K, Cu K $\alpha$   $\lambda = 1.5418$  Å). Data points show the observed PXRD pattern; the line along these points is the calculated pattern, with the difference profile at the bottom. The vertical tick marks below the pattern give the positions of the Bragg reflections.

**Table S6.** Crystallographic data for Rietveld refinement of calcined ITQ-53.

---

*PXRD data collection*

Diffraction: PANalytical X'Pert PRO

Detector: PANalytical X'Celerator

Geometry: Bragg-Bretano geometry

X-ray radiation: Cu K $_{\alpha}$  ( $\lambda_1 = 1.5406 \text{ \AA}$ ,  $\lambda_2 = 1.5444 \text{ \AA}$ ,  $I_2/I_1 = 0.5$ )

Divergence slit: fixed =  $1/16^\circ$

Goniometer arm length: 240 mm

Tube voltage and intensity: 45 kV, 40 mA

Temperature: 303 K

Scan range:  $3.0^\circ$  to  $75.0^\circ$  ( $2\theta$ ); scan step size:  $0.017^\circ$  ( $2\theta$ ); counting time: 19538 s/step.

*Crystallographic data and refinement details*

Chemical formula/unit cell: Si $_{76}$ Ge $_{76}$ O $_{300}$ (OH) $_8$

Chemical formula (Z = 152): Si $_{0.50}$ Ge $_{0.50}$ O $_{1.974}$ (OH) $_{0.053}$

Space group: *Cmcm* (no. 63)

$a = 19.0327(16) \text{ \AA}$ ;  $b = 22.6345(18) \text{ \AA}$ ;  $c = 29.252(2) \text{ \AA}$

$V = 12601.6(18) \text{ \AA}^3$ ;

$2\theta$  range =  $3-75^\circ$ ; stepsize ( $2\theta$ ) =  $0.017^\circ$

Peak range in FWHM = 9

Number of points = 4235; number of contributing reflections = 3969

Number of structural parameters = 107; number of profile parameters <sup>(a)</sup> = 13

Number of geometric restraints ( $d_{\text{Si-O}} = 1.61(1) \text{ \AA}$ ) = 43

Number of geometric restraints ( $d_{\text{Ge-O}} = 1.74(1) \text{ \AA}$ ) = 43

Number of geometric restraints ( $d_{\text{T-T}} = 3.05(1) \text{ \AA}$ ) = 23

$R_{\text{wp}} = 0.122$ ;  $R_{\text{exp}} = 0.027$ ;  $R_{\text{B}} = 0.066$ ;  $R_{\text{F}} = 0.061$

---

<sup>(a)</sup> Including zero-shift and unit cell parameters.

**Table S7.** Atomic coordinates, atomic displacement parameters and occupancy for calcined ITQ-53.

T-site	Atom	x <sup>(a)</sup>	y <sup>(a)</sup>	z <sup>(a)</sup>	U <sub>iso</sub> <sup>(b)</sup>	Occupancy <sup>(a,c)</sup>	Multiplicity & Wyckoff
Si1	Si	0.1364(3)	0.2955(3)	0.45342(18)	0.0370(7)	0.0	16h
Ge1	Ge	0.1364(3)	0.2955(3)	0.45342(18)	0.0370(7)	1.0	16h
Si2	Si	0.3669(3)	0.2412(3)	0.4439(2)	0.0370(7)	0.36(3)	16h
Ge2	Ge	0.3669(3)	0.2412(3)	0.4439(2)	0.0370(7)	0.64(3)	16h
Si3	Si	0.2228(3)	0.1828(2)	0.4362(2)	0.0370(7)	0.39(3)	16h
Ge3	Ge	0.2228(3)	0.1828(2)	0.4362(2)	0.0370(7)	0.61(3)	16h
Si4	Si	0.2195(3)	0.1473(3)	0.5388(2)	0.0370(7)	0.64(3)	16h
Ge4	Ge	0.2195(3)	0.1473(3)	0.5388(2)	0.0370(7)	0.36(3)	16h
Si5	Si	0.1278(3)	0.0846(3)	0.4001(2)	0.0370(7)	0.69(3)	16h
Ge5	Ge	0.1278(3)	0.0846(3)	0.4001(2)	0.0370(7)	0.31(3)	16h
Si6	Si	0.1369(4)	0.0316(2)	0.5463(2)	0.0370(7)	0.59(2)	16h
Ge6	Ge	0.1369(4)	0.0316(2)	0.5463(2)	0.0370(7)	0.41(2)	16h
Si7	Si	0.0801(3)	0.1113(3)	0.30221(17)	0.0370(7)	0.614(18)	16h
Ge7	Ge	0.0801(3)	0.1113(3)	0.30221(17)	0.0370(7)	0.386(18)	16h
Si8	Si	0	0.2699(3)	0.4023(2)	0.0370(7)	0.38(4)	8f
Ge8	Ge	0	0.2699(3)	0.4023(2)	0.0370(7)	0.62(4)	8f
Si9	Si	0	0.2141(3)	0.6040(2)	0.0370(7)	0.68(4)	8f
Ge9	Ge	0	0.2141(3)	0.6040(2)	0.0370(7)	0.32(4)	8f
Si10	Si	0	0.1454(3)	0.44421(20)	0.0370(7)	0.74(3)	8f
Ge10	Ge	0	0.1454(3)	0.44421(20)	0.0370(7)	0.26(3)	8f
Si11	Si	0	0.1038(3)	0.5438(2)	0.0370(7)	0.86(4)	8f
Ge11	Ge	0	0.1038(3)	0.5438(2)	0.0370(7)	0.14(4)	8f
Si12	Si	0	0.2294(3)	0.30214(17)	0.0370(7)	0.26(3)	8f
Ge12	Ge	0	0.2294(3)	0.30214(17)	0.0370(7)	0.74(3)	8f
O1	O	0.200(2)	0.126(3)	0.402(2)	0.0413(20)	1	16h
O2	O	0.0816(12)	0.0874(14)	0.555(2)	0.0413(20)	1	16h
O3	O	0.230(4)	0.1388(12)	0.4827(4)	0.0413(20)	1	16h
O4	O	0.0830(18)	0.298(4)	0.4051(10)	0.0413(20)	1	16h
O5	O	0.299(2)	0.210(4)	0.4142(7)	0.0413(20)	1	16h
O6	O	0.175(5)	0.242(3)	0.4179(5)	0.0413(20)	1	16h
O7	O	0.201(3)	0.0800(17)	0.558(2)	0.0413(20)	1	16h
O8	O	0.205(2)	0.340(4)	0.4337(17)	0.0413(20)	1	16h
O9	O	0.325(5)	0.305(2)	0.4285(8)	0.0413(20)	1	16h
O10	O	0.0466(13)	0.109(3)	0.4069(13)	0.0413(20)	1	16h
O11	O	0.120(4)	0.074(2)	0.3441(5)	0.0413(20)	1	16h
O12	O	0.4473(19)	0.2372(10)	0.420(3)	0.0413(20)	1	16h
O13	O	0.1648(10)	0.972(2)	0.574(3)	0.0413(20)	1	16h

O14	O	0.109(3)	0.301(2)	0.5105(5)	0.0413(20)	1	16h
O15	O	0.0746(5)	0.1857(4)	0.300(3)	0.0413(20)	1	16h
O16	O	0.111(3)	0.097(5)	¼	0.0413(20)	1	8g
O17	O	0	0.1486(8)	0.5002(3)	0.0413(20)	1	8f
O18	O	0	0.1735(6)	0.5575(6)	0.0413(20)	1	8f
O19	O	0	0.0795(4)	0.304(5)	0.0413(20)	1	8f
O20	O	0	0.2810(7)	0.3450(3)	0.0413(20)	1	8f
O21	O	0	0.1953(5)	0.4041(6)	0.0413(20)	1	8f
O22	O	0.1700(13)	0	½	0.0413(20)	1	8e
O23	O	0	0.2638(10)	¼	0.0413(20)	1	4c
OH1	O	0	0.180(4)	0.6540(19)	0.050(3)	1	8f

Numbers in parentheses are the esd's in the units of the least significant digit given.

<sup>(a)</sup> Parameters without an esd were not refined. Coordinates equal to 0, ¼ or ½ are fixed by symmetry. <sup>(b)</sup> All the Si atoms have been refined with a common  $U_{\text{iso}}$  parameter; the same applies for all the O atoms. <sup>(c)</sup> Total occupancy of each T-site is constrained to be equal to 1.

**Table S8.** Interatomic bond distances T-O (in Å) for calcined ITQ-53.

Tx-	-O <sub>x<sub>a</sub></sub>	-O <sub>x<sub>b</sub></sub>	-O <sub>x<sub>c</sub></sub>	-O <sub>x<sub>d</sub></sub>	$d_{\text{(T-O)}}^{(a)}$	$d_{\text{(T-O)}}^{(b)}$	Occ <sub>Ge</sub> <sup>(c)</sup>
T1-	-O4=1.742(32)	-O8=1.747(62)	-O14=1.754(23)	-O6=1.757(62)	1.750	1.74	1.00
T2-	-O12=1.685(49)	-O14=1.704(32)	-O5=1.710(49)	-O9=1.710(59)	1.702	1.69	0.64
T3-	-O1=1.686(63)	-O3=1.691(20)	-O5=1.702(47)	-O6=1.706(74)	1.696	1.69	0.61
T4-	-O7=1.661(43)	-O3=1.664(16)	-O8=1.672(44)	-O9=1.673(58)	1.668	1.66	0.36
T5-	-O13=1.647(55)	-O10=1.653(33)	-O11=1.662(18)	-O1=1.664(50)	1.657	1.65	0.31
T6-	-O22=1.656(11)	-O13=1.661(57)	-O2=1.664(30)	-O7=1.675(51)	1.664	1.66	0.41
T7-	-O16=1.668(30)	-O11=1.671(43)	-O19=1.687(8)	-O15=1.689(12)	1.679	1.66	0.39
T8-	-O21=1.689(13)	-O20=1.695(11)	-O4=1.705(46)	-O4=1.705(46)	1.699	1.69	0.62
T9-	-O18=1.642(18)	-O12=1.647(46)	-O12=1.647(46)	-OH1=1.654(65)	1.648	1.65	0.32
T10-	-O21=1.629(16)	-O10=1.630(45)	-O10=1.630(45)	-O17=1.639(11)	1.632	1.64	0.26
T11-	-O18=1.628(15)	-O17=1.629(15)	-O2=1.630(26)	-O2=1.630(26)	1.629	1.63	0.14
T12-	-O23=1.713(12)	-O20=1.714(14)	-O15=1.732(11)	-O15=1.732(11)	1.723	1.71	0.74

(a) Average values; (b) calculated theoretical values ( $d_{\text{Si-O}} = 1.61$  Å,  $d_{\text{Ge-O}} = 1.74$  Å); (c) Ge occupancies.

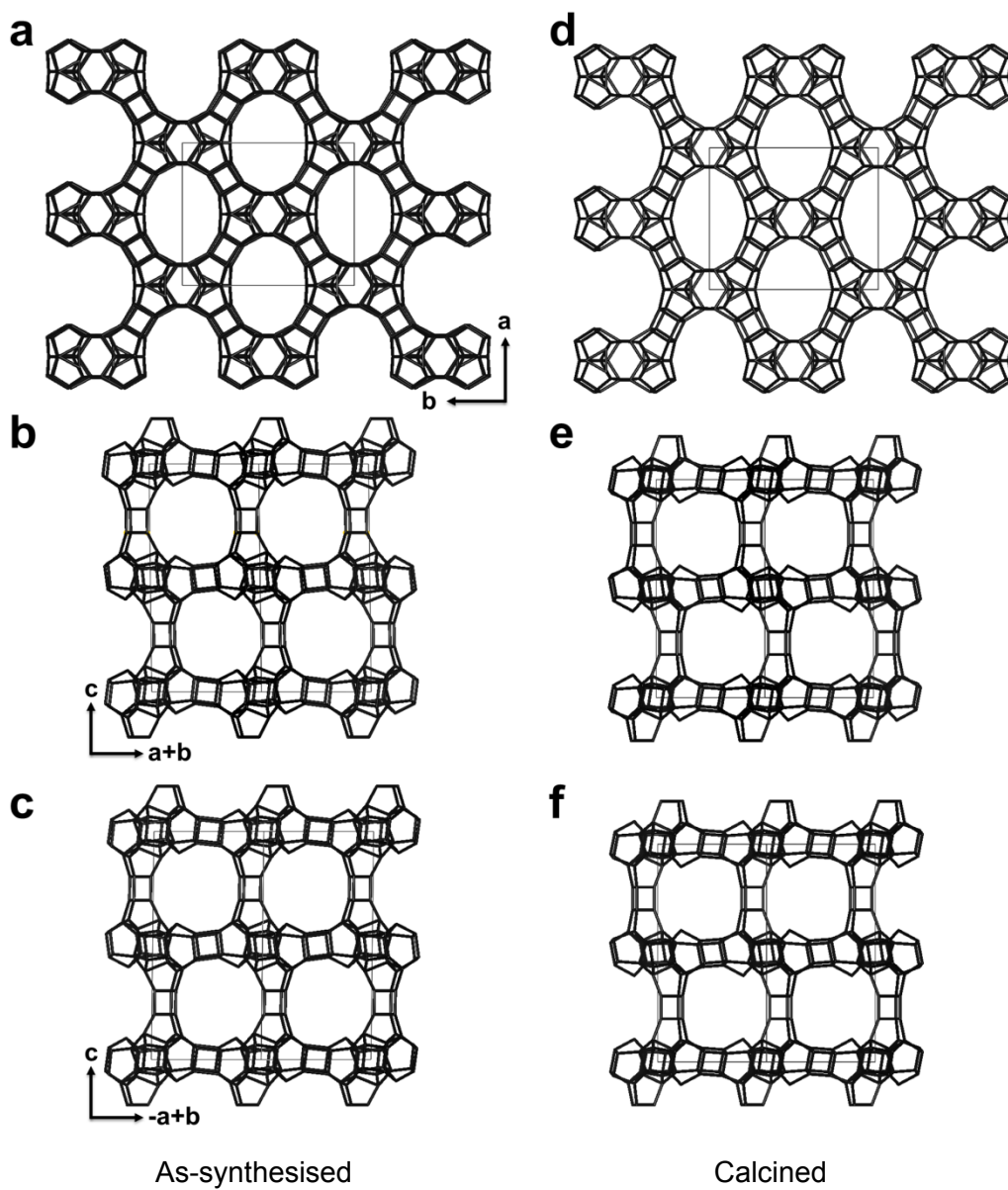


**Figure S7.** Comparison of the refined structure models of (a-c) as-synthesised and (d-f) calcined ITQ-53 viewed along the (a, d) [001], (b, e) [1-10] and (c, f) [110] directions. Only the T-T connections are shown for clarity.

### S8. Topology analysis of the ITQ-53 framework

Topology analysis of the ITQ-53 framework was performed using *TOPOS*<sup>4</sup>. The visualisation of nets and tiling was generated using *3dt*<sup>5</sup>.

**Table S9.** Coordination sequences and vertex symbols of ITQ-53

T-atom name	N1 to N10	Vertex Symbol
T1	4 9 16 22 37 48 69 94 127 159	4.5.4.6(2).4.14(3)
T2	4 8 15 25 34 46 67 100 131 152	4.5.4.6(2).4.14
T3	4 9 15 23 35 49 71 96 124 154	4.5.4.5.4.14
T4	4 9 16 28 30 46 72 104 128 153	4.5.4.5.4.14(3)
T5	4 12 18 23 36 55 73 102 125 147	5.5(2).5.14.5.16
T6	4 12 20 24 33 49 76 106 128 153	5.5(2).5.6.5.14(2)
T7	4 8 15 27 36 47 73 104 123 147	3.14.4.5.4.5
T8	4 12 16 22 39 62 69 96 128 155	5.14.5.14.5(2).6
T9	3 9 15 23 36 42 66 101 128 152	Rings coincide with circuits
T10	4 12 16 21 31 53 83 91 123 142	Rings coincide with circuits
T11	4 11 19 24 28 49 78 105 125 154	Rings coincide with circuits
T12	4 8 14 23 36 53 80 98 108 142	3.14(2).4.5.4.5

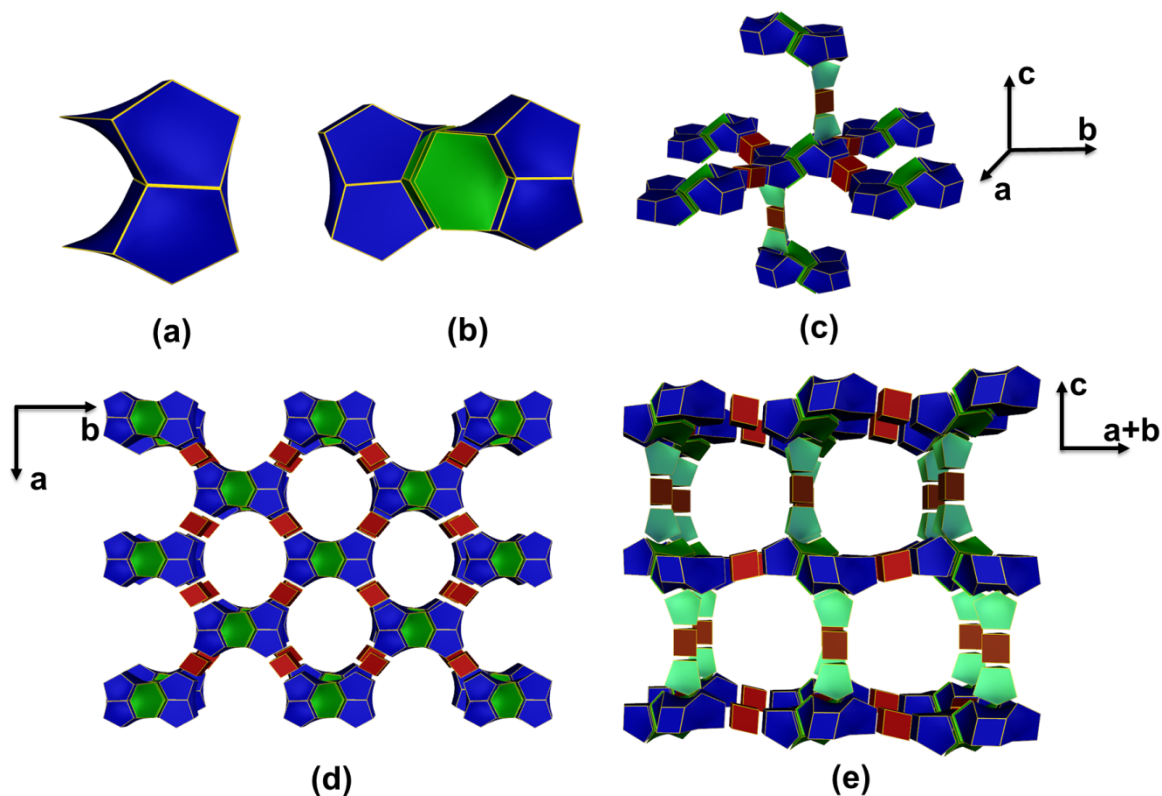


**Figure S8.** Construction of the structure of ITQ-53 using tiling. (a) The new [4<sup>2</sup>5<sup>8</sup>6] composite building unit (CBU, in blue). (b) Connectivity of the [4<sup>2</sup>5<sup>8</sup>6] CBU to another CBU via two [5<sup>2</sup>6<sup>2</sup>] tiles (in green). (c) Each unit in (b) connects to other six similar units; four of them via [4<sup>6</sup>] tiles (D4Rs in red) in *ab* plane and the other two via two [3<sup>1</sup>5<sup>3</sup>] (in light green) and one [3<sup>2</sup>4<sup>3</sup>] (D3R, in brown) tiles along the *c*-axis. (d) The double layer with 14-ring pores. (e) The 14-ring double layers in (d) connect to each other via [3<sup>1</sup>5<sup>3</sup>], [3<sup>2</sup>4<sup>3</sup>] and [3<sup>1</sup>5<sup>3</sup>] tiles along *c*-axis to form the 3D framework of ITQ-53, as viewed along (e) [1-10] (equivalent to [110]) showing the 14-ring channels parallel to the double layers.

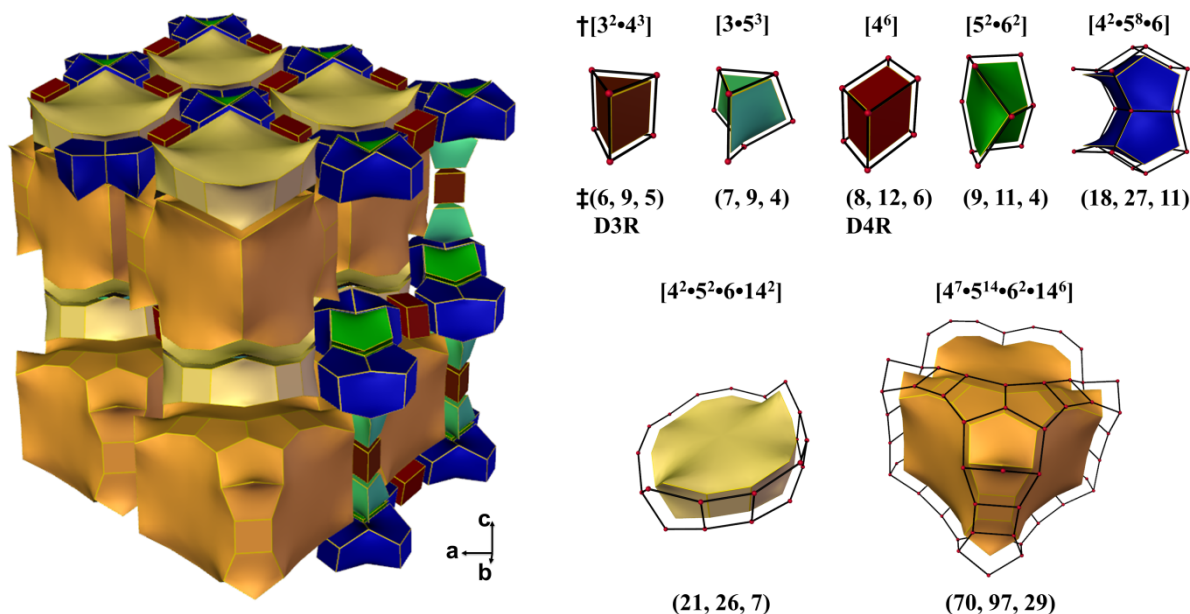


**Figure S9.** Illustration of the channel system in ITQ-53 using tiling. Two large tiles,  $[4^2.5^2.6.14^2]$  and  $[4^7.5^{14}.6^2.14^6]$  represent the cavities in ITQ-53. Each  $[4^7.5^{14}.6^2.14^6]$  cavity connects to two  $[4^7.5^{14}.6^2.14^6]$  along  $[1-10]$  and connects to other two  $[4^7.5^{14}.6^2.14^6]$  along  $[110]$  via 14-ring windows. Along the  $c$ -axis, each  $[4^7.5^{14}.6^2.14^6]$  tile connects to two  $[4^7.5^{14}.6^2.14^6]$  via bridging  $[4^2.5^2.6.14^2]$  tiles by sharing 14-ring windows. The seven different tiles in ITQ-53 are shown on the right. †[Face symbol], ‡(V, E, F): number of vertices, number of edges, number of faces. \*Tiling signature:  $[3^2.4^3] + 2[3.5^3] + 2[4^6] + [4^7.5^{14}.6^2.14^6] + 2[4^2.5^8.6] + 2[4^2.5^2.6.14^2] + 2[5^2.6^2]$ . The transitivity of the ITQ-53 framework based on the T-atoms is **12 23 18 7**.

## References

1. W. Wan, J. Sun, J. Su, S. Hovmoller, and X. Zou, *J. Appl. Crystallogr.*, 2013, **46**, 1863–1873.
2. G. M. Sheldrick, *Acta Crystallogr. A*, 2008, **64**, 112–122.
3. R. A. Young and R. A. Young, *The Rietveld Method*, Oxford University Press, 1995.
4. V. A. Blatov, *Struct. Chem.*, 2012, **23**, 955–963.
5. O. Delgado-Friedrichs, *Theor. Comput. Sci.*, 2003, **303**, 431–445.